Power Flow Maximization in Permanent-Magnet Generators

Guillermo R. Catuogno, *Student Member, IEEE*, Daniel G. Forchetti, Roberto Leidhold, *Member, IEEE*, and Guillermo O. Garcia, *Senior Member, IEEE*

***Abstract*—The main hypothesis proposed in this paper is that by controlling the harmonic and zero-sequence components of the current in nonsinusoidal permanent-magnet synchronous generators (PMGs), additional energy can be obtained, thereby increasing the machine power density without increasing the Joule effect losses. Two different strategies are proposed for three- and four-wire topologies; therefore, four different cases are analyzed. The strategies consist in controlling the PMG stator currents, following a function that depends on the waveform of the back electromotive force (EMF). The current function is obtained from the instantaneous reactive power theory. An experimental system was built to validate the proposal. Experimental results prove that it is possible to increase power in a tested PMG by 7% using the four-wire topology in comparison with the conventional block commutation and same losses. Higher power gain can be obtained for machines with almost rectangular-shaped EMF waveforms.**

***Index Terms*—Four-wire topologies, permanent-magnet (PM) machines, power control.**

I. Introduction

PERMANENT-MAGNET synchronous generators (PMGs) are characterized by high power density due to the presence of high-energy magnets, for instance, neodymium–iron–boron (NeFeB) or samarium–cobalt (SmCo), commonly used to construct them. They can be also built with a high number of poles, which enables them to work at low speed. For these reasons, they are suitable for direct-driven wind energy systems [1]–[3]. PMGs usually operate at variable speed, and power flow control is carried out by imposing the waveform and amplitude of the stator currents using a power electronic converter [4], [5].

While the waveform of the electromotive force (EMF) of a PMG can have an arbitrary number of constituent harmonics, the most common classification is sinusoidal or trapezoidal [6], [7].

Sinusoidal PMGs: In this type of machines, the stator currents have to be sinusoidal and synchronized with the rotor in order to produce a ripple-free torque. This is the case of the conventional field-oriented control. Moreover, to obtain a good control of torque, it is necessary to know the rotor angular position accurately to synchronize the stator currents [8].

Trapezoidal PMGs: In these machines, usually named brushless dc machines, the torque control is carried out by imposing constant current in the intervals at which the EMF is also constant. Therefore, it is necessary to know the rotor angles for which the EMF shape changes (usually six angles). This control strategy is known as block commutation, which has been very popular due to its simple implementation. In practice, it is very difficult to obtain an ideal trapezoidal waveform, i.e., having a flat top for a span of 120°. Due to this, and the fact that currents require some slope while commutating, trapezoidal PMGs usually present a significant electromagnetic torque ripple [9]–[12].

A PMG neither sinusoidal nor trapezoidal needs to be fed with a particular current waveform to avoid electromagnetic torque ripple. In order to reduce the torque ripple, some authors [13], [14] proposed strategies based on the harmonics injection method to generate the reference values of the stator currents [15].

Other authors proposed strategies based on the instantaneous reactive power theory [16] to generate the current references to avoid torque ripple in machines with arbitrary EMF waveforms [17].

In most cases, PMGs are machines with three star-connected windings; thus zero-sequence current cannot circulate. The main hypothesis proposed in this paper is that by controlling the current harmonic components, including the zero-sequence component, additional power can be generated without increasing the losses, thereby increasing the machine's power density.

Some authors proposed the use of zero-sequence currents in machines with more than three phases, such as in [18]–[20]. In [21], the zero-sequence current is used to produce torque, which was tested by simulation. However, only the third harmonic is used in this case; thus, no advantage is taken from other harmonic components.

It is suitable for the control strategies proposed in this paper that almost rectangular-shaped waveforms, i.e., with high harmonic content, are considered to design the generator. For these waveforms, the high form factor and zero-sequence component of the EMF contribute in increasing the generated power. On

Manuscript received September 10, 2013; revised December 20, 2013; accepted February 24, 2014. Date of publication April 9, 2014; date of current version September 12, 2014. This work was supported in part by the Universidad Nacional de Río Cuarto, in part by Otto-von-Guericke-Universitaet Magdeburg, in part by the Fondo para la Investigación Científica y Tecnológica–Agencia Nacional de Promoción Científica y Tecnológica, and in part by the Consejo Nacional de Investigaciones Científicas y Técnicas.

G. R. Catuogno, D. G. Forchetti, and G. O. Garcia are with the Grupo de Electrónica Aplicada, Facultad de Ingeniería, Universidad Nacional de Río Cuarto, X5804BYA Río Cuarto, Argentina; and also with the Consejo Nacional de Investigaciones Científicas y Técnicas, C1033AAJ Buenos Aires, Argentina (e-mail: grcatu@ieee.org; dforchetti@gmail.com; ggarcia@ieee.org).

R. Leidhold is with the Institute for Electric Power Systems, Otto-von-Guericke-Universitaet Magdeburg, 39106 Magdeburg, Germany (e-mail: roberto.leidhold@ovgu.de).

Color versions of one or more of the figures in this paper are available online at http://ieeexplore.ieee.org.

Digital Object Identifier 10.1109/TIE.2014.2316269

the contrary, a generator with sinusoidal EMF cannot generate additional power.

In this paper, two control strategies are proposed to maximize the average power generated by a PMG. These strategies consist in controlling the stator currents, including the zero-sequence component. The reference values of these currents are calculated using an algorithm deduced from the instantaneous reactive power theory. The implementation of the algorithm requires a converter to control the stator currents. Two different converter topologies to feed the four-wire machine were explored and evaluated. The first one consists of a four-leg converter (4wEL), and the second one consists of a three-leg converter plus the middle point of a dc-link capacitor bank (4wDC) [21].

The connection of the neutral point of the generator allows the possibility of implementing a reconfigurable fault-tolerant system [22]–[25], but this is not discussed in this paper.

This paper is organized as follows. Section II presents the PMG model. Two different PMG power flow control strategies, including the calculation of the reference values of stator currents and a block diagram for a practical implementation, are proposed in Section III. The experimental results that validate the proposed strategies that were obtained using a prototype are given in Section IV. Finally, conclusions are drawn in Section V.

II. PMG Model

A PMG can be represented by the following model in abc variables [21]:

$$\vec{v}_{abcn} = r_s \vec{i}_{abc} + \mathbf{L}\frac{d}{dt}\vec{i}_{abc} + \vec{e}_{abc} \tag{1}$$

$$i_n = i_a + i_b + i_c \tag{2}$$

where $\vec{v}_{abcn}$, $\vec{i}_{abc}$, and $\vec{e}_{abc}$ are the voltages, currents, and EMFs of the stator phases, respectively; i_n is the neutral current; r_s is the resistance of the stator windings; $\mathbf{L}$ is the stator inductance matrix, which is composed of the phase inductances L_s in the diagonal and by the mutual inductances M in the other components. Thus,

$$\vec{v}_{abcn} = [\, v_{an} \quad v_{bn} \quad v_{cn} \,]^T$$
$$\vec{i}_{abc} = [\, i_a \quad i_b \quad i_c \,]^T$$
$$\vec{e}_{abc} = [\, e_a \quad e_b \quad e_c \,]^T$$

with

$$e_j = \frac{d\psi_j}{dt} = \frac{d\psi_j}{d\theta}\frac{d\theta}{dt} = \varphi_j(\theta)\omega, \qquad j = a, b, c \tag{3}$$

where ψ_j are the rotor fluxes linked by the stator, ω is the rotor angular speed ($d\theta/dt = \omega$), and $\varphi_j(\theta)$ are functions that determine the waveform of the EMF. These functions depend on the geometric distribution of the stator windings, as well as on the shape and features of both the magnets and the stator magnetic core.

To simplify the model, the following transformation is used:

$$\vec{f}_{\alpha\beta0} = \mathbf{K}\vec{f}_{abc} \quad \vec{f}_{\alpha\beta0} = [\, f_\alpha \quad f_\beta \quad f_0 \,]^T \quad \vec{f}_{abc} = [\, f_a \quad f_b \quad f_c \,]^T$$
$$\mathbf{K} = \frac{2}{3}\begin{bmatrix} 1 & -1/2 & -1/2 \\ 0 & \sqrt{3}/2 & -\sqrt{3}/2 \\ 1/2 & 1/2 & 1/2 \end{bmatrix} \tag{4}$$

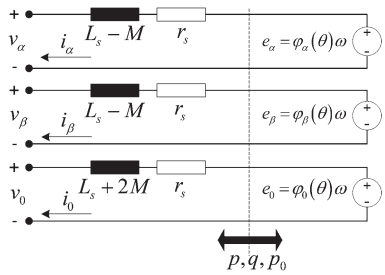

Fig. 1. Equivalent circuit of the PMG in the $\alpha\beta0$ reference frame.

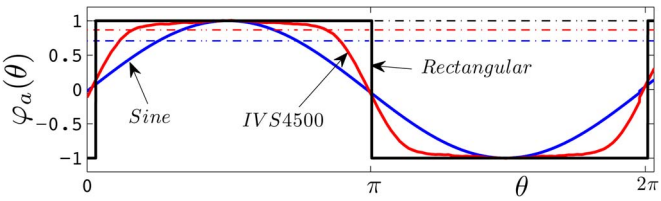

Fig. 2. (Solid) EMF waveform and (dashed) RMS value for the following cases: (blue) sinusoidal, (red) generator IVS4500, and (black) ideal rectangular.

where $\vec{f}$ is a generic variable of the model (flux, current, voltage, or EMF). Thereafter, the PMG model in $\alpha\beta0$ variables can be described by the following equations:

$$\vec{v}_{\alpha\beta0} = r_s \vec{i}_{\alpha\beta0} + \boldsymbol{L_0}\frac{d}{dt}\vec{i}_{\alpha\beta0} + \vec{e}_{\alpha\beta0} \tag{5}$$

where $\vec{v}_{\alpha\beta0}$, $\vec{i}_{\alpha\beta0}$, and $\vec{e}_{\alpha\beta0}$ are the voltage, current, and EMF in $\alpha\beta0$ variables, respectively. $\boldsymbol{L_0}$ is the transformed inductance matrix composed of $\boldsymbol{L_0} = \mathrm{diag}[L_s - M, L_s - M, L_s + 2M]$. By inspection of (5), the equivalent circuit shown in Fig. 1 can be proposed.

Equation (3), which defines the EMFs, can be written in variables $\alpha\beta0$ as follows:

$$\vec{e}_{\alpha\beta0} = \omega\,[\, \varphi_\alpha(\theta) \quad \varphi_\beta(\theta) \quad \varphi_0(\theta) \,]^T. \tag{6}$$

Is important to note that the shape of the EMF waveform determines the power density of the PMGs [26]. In Fig. 2, three cases can be observed: the ideal sinusoidal waveform with an RMS value of $1/\sqrt{2}$ p.u., the waveform of the generator IVS4500 described in Section III-B with an RMS value of 0.866 p.u., and the ideal rectangular waveform with the maximum possible RMS value of 1 p.u.

III. Power Flow Analysis and Control

The control strategies proposed in this paper are based on the instantaneous reactive power theory [16]. This theory states that, in a three-phase electrical system, the following instantaneous power components can be identified:

$$p = \bar{p} + \tilde{p}$$
$$q = \bar{q} + \tilde{q}$$
$$p_0 = \bar{p}_0 + \tilde{p}_0. \tag{7}$$

p is the instantaneous active or real power, q is the instantaneous reactive or imaginary power, and p_0 is the instantaneous homopolar power. Each of them can be decomposed in the mean term, designated by an overline $(-)$, and the oscillatory term, designated by a tilde $(\sim)$.

The components of the instantaneous reactive power, i.e., $\bar{q}$ and $\tilde{q}$, represent the energy exchanged between the electrical phases. They do not contribute to the energy transfer from the generator. These components represent a power flow that stores energy in nondissipative components (inductors and capacitors). They do not produce mechanical torque in the generator shaft, but they do produce losses. Therefore, it is desirable to eliminate or at least minimize them.

The oscillatory components $\tilde{p}$ and $\tilde{p_0}$ do not contribute to the mean energy transfer from the generator, but they represent an oscillatory exchange of energy that produces oscillatory mechanical torque in the generator shaft. Then, it is also desirable to eliminate or at least minimize them to avoid mechanical stress.

The power components $\bar{p}$ and $\bar{p_0}$ represent the mean power flow from the generator. Therefore, it is desirable to maximize the sum of these two components in order to maximize the energy transferred from the generator.

It is important to notice that the continuous component of the instantaneous homopolar power, i.e., $\bar{p_0}$, cannot exist in absence of the oscillatory component $\tilde{p_0}$ [16]. Therefore, maximizing the homopolar component $\bar{p_0}$ implies that an oscillatory component $\tilde{p_0}$ must be accepted and, consequently, an oscillatory torque in the generator shaft.

It will be demonstrated in this paper that it is possible to compensate the torque oscillation produced by the homopolar component $\tilde{p_0}$ by adequately controlling the oscillatory active component $\tilde{p}$.

In conclusion, the following control objectives can be stated: by controlling the instantaneous power components, the following is possible.

1) Maximize the total power P_T transferred from the generator by maximizing the following expression:

$$P_T = (\bar{p} + \tilde{p}) + (\bar{p_0} + \tilde{p_0}). \tag{8}$$

2) Minimize losses minimizing the following expression:

$$q = \bar{q} + \tilde{q}. \tag{9}$$

3) Minimize the torque ripple by minimizing the following expression:

$$P_{\text{osc}} = \tilde{p} + \tilde{p_0}. \tag{10}$$

Once the control objectives are defined, it is necessary to determine which variables can be manipulated to fulfill them.

It can be demonstrated that the instantaneous power components can be expressed in terms of the phase currents as follows [16]:

$$\begin{aligned} p &= \frac{3}{2}(e_\alpha i_\alpha + e_\beta i_\beta) \\ q &= \frac{3}{2}(e_\alpha i_\beta - e_\beta i_\alpha) \\ p_0 &= 3 e_0 i_0. \end{aligned} \tag{11}$$

Equation (11) suggests that it is possible to control the instantaneous power components by imposing the PMG stator currents using a power electronic converter.

A method to calculate the reference values for the stator currents able to achieve the control objectives is proposed in the following section.

A. Determination of the Reference Values for Stator Currents

The main purpose of this paper is to control the instantaneous power components by imposing the adequate stator currents, in order to reach the control objectives. The proposed strategies can be treated as an optimization problem; therefore, the Lagrange multiplier method [27] will be used to solve these problems.

For each strategy, we define the following:

1) the objective or the function to be optimized, as $f(\vec{x})$;
2) the restrictions, as $g(\vec{x}) = 0$;
3) the free variables, as $\vec{x}$.

This method consists in building a function $h(\vec{x}, \lambda)$ as follows:

$$h(\vec{x}, \lambda) = f(\vec{x}) - \lambda\left(g(\vec{x})\right). \tag{12}$$

The PMG mechanical and core losses are not considered in the following deductions because they are almost not influenced by the free variables (the stator currents). In permanent-magnet (PM) machines with surface-mounted magnets, the flux in the stator core is mainly due to the PMs. The air gap and the low permeability of the magnets count for a relatively high reluctance path, and thus, the stator current contributes only marginally to the flux. Consequently, the core losses mainly depend on the machine design and the speed, but the influence of the current waveform can be neglected.

1) Strategy 1 (Losses Minimization With Ripple-Free Torque Restriction):

- Objective: minimize the PMG losses.
- Restriction: eliminate electromagnetic torque ripple.
- Free variables: stator currents.

The problem can be mathematically enunciated as follows:

$$\begin{aligned} f(i_\alpha, i_\beta, i_0): &\quad P_{cu} = \frac{3}{2} R\left(i_\alpha^2 + i_\beta^2 + i_0^2\right) \\ g(i_\alpha, i_\beta, i_0): &\quad P_T = p + p_0 = \frac{3}{2}(e_\alpha i_\alpha + e_\beta i_\beta) + 3 e_0 i_0. \end{aligned} \tag{13}$$

From (6) and the equation system that results from $\vec{\nabla} h(\vec{x}, \lambda) = \vec{0}$, it is possible to solve the equations for the stator current $(\vec{i}^*_{\alpha\beta 0})$ as follows:

$$\begin{aligned} i_\alpha^* &= \frac{2}{3}\frac{1}{\omega \Delta_{4w}} \varphi_\alpha(\theta) P_T^* \\ i_\beta^* &= \frac{2}{3}\frac{1}{\omega \Delta_{4w}} \varphi_\beta(\theta) P_T^* \\ i_0^* &= \frac{2}{3}\frac{1}{\omega \Delta_{4w}} \varphi_0(\theta) P_T^* \end{aligned} \tag{14}$$

where

$$\Delta_{4w} = \left[\varphi_\alpha^2(\theta) + \varphi_\beta^2(\theta) + 2\varphi_0^2(\theta)\right]. \tag{15}$$

The proposed method allows finding the reference currents required to achieve a constant total power. In addition, by using these references, the power is optimally shared between p and

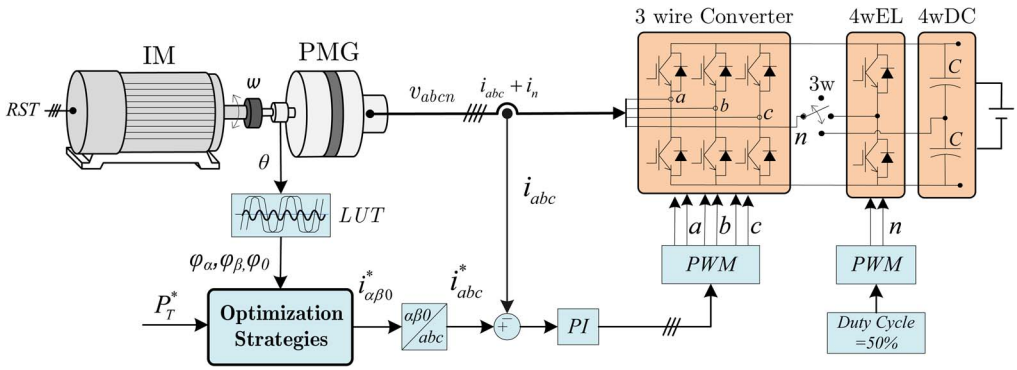

Fig. 3. Simplified block diagram of the implemented prototype.

p_0, and the reactive power is $q = 0$. The latter can be made explicit by replacing the references (14) and the EMF (6) into the reactive power in (11).

The practical implementation of this strategy imposes a four-wire power electronic converter to control the current of the three phases, including the zero-sequence component.

2) Strategy 2 (Maximization of the Total Power With Thermal Limit Restriction):

- Objective: maximize the generated energy.
- Restriction: machine thermal limit of operation (P_{cu}).
- Free variables: stator currents.

The problem can be mathematically enunciated as follows:

$$\begin{aligned} f(i_\alpha, i_\beta): \quad & P_T = p + p_0 = \frac{3}{2}(e_\alpha i_\alpha + e_\beta i_\beta) + 3e_0 i_0 \\ g(i_\alpha, i_\beta): \quad & P_{cu} = \frac{3}{2} R \left(i_\alpha^2 + i_\beta^2 + i_0^2\right). \end{aligned} \tag{16}$$

From (6) and the equation system that results from $\vec{\nabla} h(\vec{x}, \lambda) = \vec{0}$, it is possible to solve the equations for the stator current $(\vec{i}^*_{\alpha\beta 0})$ as follows:

$$\begin{aligned} i^*_\alpha &= \varphi_\alpha(\theta)\sqrt{\frac{2P_{cu}}{3\Delta_{4w}}} \\ i^*_\beta &= \varphi_\beta(\theta)\sqrt{\frac{2P_{cu}}{3\Delta_{4w}}} \\ i^*_0 &= \varphi_0(\theta)\sqrt{\frac{2P_{cu}}{3\Delta_{4w}}}. \end{aligned} \tag{17}$$

In this case, the proposed method allows obtaining the reference currents required to achieve the maximum generated energy, disregarding the ripple. Here again, power is optimally shared between p and p_0 for the new objective, and the reactive power is $q = 0$. The latter can be made explicit by replacing the references (17) and the EMF (6) into the reactive power (11).

The practical implementation of this strategy imposes a four-wire power electronic converter to control the three phases plus the neutral currents.

B. Practical Implementation

In order to implement the control strategies proposed in the previous section, an experimental prototype was built (see Fig. 3).

The experimental prototype has a four-wire PMG (three phases plus neutral) connected to either a four-leg inverter (4wEL) or a three-leg inverter plus of the middle point of a dc-link capacitor bank (4wDC). The PMG is an IVS4500 available in our laboratory. Table I shows the main parameters of this generator, and Fig. 4 shows the functions $\varphi_{\alpha\beta 0}$ experimentally obtained at rated speed for the generator with no load, by measuring the stator voltages as a function of the position and dividing them by the speed [based on (3)].

TABLE I
PMG PARAMETERS

Parameter	Value
P	$5\,kW$
Poles	16
ω_n	$600\,rpm$
r_s	$0.215\,\Omega$
L_s	$1.12\,mH$
$Slots$	48
v_f	$48\,V$
f	$80\,Hz$
$Magnets$	$Ferrite$
$Windings$	$Distributed$

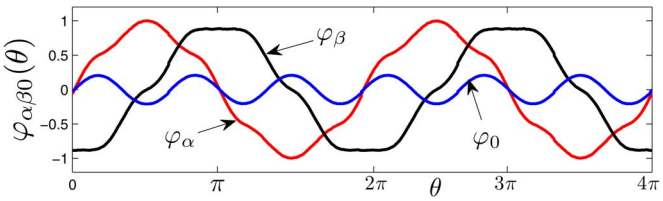

Fig. 4. Waveform of $\varphi_{\alpha\beta 0}(\theta)$ in the $\alpha\beta 0$ reference frame.

The generator parameters were experimentally obtained by performing open- and short-circuit tests.

A speed-controlled prime mover drives the generator. The four-leg inverter (4wEL) is actuated by a pulsewidth modulator (PWM). The inverter was implemented using insulated gate bipolar transistors switching at 25 kHz. The controller was implemented with a Texas Instruments digital signal processor TMS320F28335 working at 150 MHz. The sampling frequency of the control algorithm was 25 kHz and synchronized with the PWM. The PMG shaft position is sensed by using an optical encoder with 1024 pulses per turn.

As it was shown before, the proposed strategies require knowing the functions $\varphi_{\alpha\beta 0}(\theta)$, which can be experimentally obtained. These functions were stored in a lookup table indexed by the rotor position, as shown in Fig. 4.

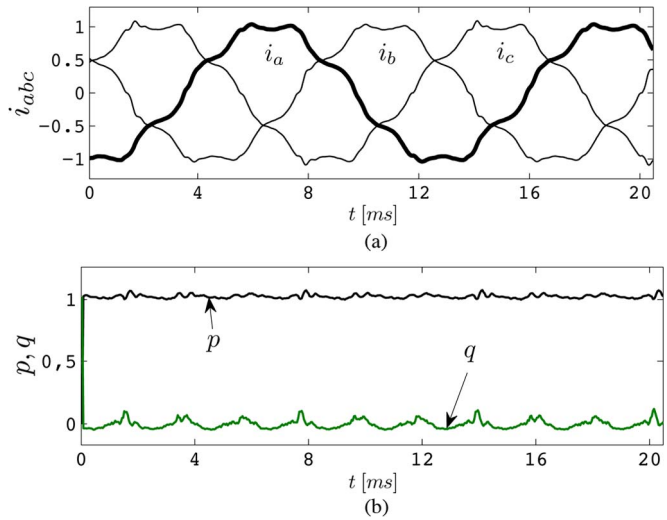

Fig. 5. Currents and power components for Case 1: Strategy 1 and three-wire topology (experimental data). (a) Measured currents. (b) Power components.

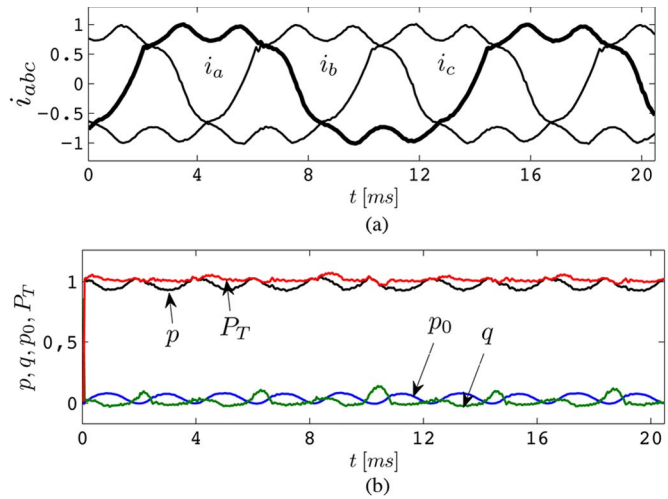

Fig. 6. Currents and power components for Case 2: Strategy 1 and four-wire topology (experimental data). (a) Measured currents. (b) Power components.

The block Optimization Strategies shown in Fig. 3 represents the algorithm (14) or (17) that generates the stator current reference values. Fig. 3 also shows the blocks and signals that represent the fast current control loop of the stator currents.

As it was stated, it is possible to implement an alternative topology using a three-leg inverter while connecting the neutral of the PMG to the midpoint of the dc-link capacitor bank (4wDC), instead of using a fourth inverter leg.

IV. Experimental Results

The control Strategies 1 and 2 proposed in Section III-A were tested in the prototype described in Section III-B, and some experimental results are presented in this section.

Topologies 4wEL and 4wDC produced the same results at rated speed, as it was validated experimentally; therefore, only results of one topology are shown in this paper.

Moreover, results obtained using the proposed strategies with a conventional three-leg inverter are also shown to compare them with those of the four-wire topologies.

In the following sections, first, the evolution of variables or temporal analysis and then a comparative analysis of the studied cases are presented.

In all the tests, the PMG runs at constant speed, i.e., $\omega = 1$ p.u., and the dc-link voltage stays at its nominal value, i.e., Vdc $= 1$ p.u.

The base value for power is the one that produces the rated losses using the standard block commutation.

A. Experimental Results

1) Case 1—Strategy 1 in a Three-Wire Topology (Losses Minimization With Ripple-Free Torque Restriction): In Fig. 5(a), the measured currents in abc variables can be observed. These currents are necessary to obtain the constant total power P_T.

Fig. 5(b) shows the waveforms of the power components for this case. It can be observed that, as a result of applying the proposed control strategy, the reactive power q is null, and due to the absence of neutral connection, the homopolar power p_0 is also null.

From the same figure, it can be concluded that the total power P_T is 1.03 p.u., constant, and equal to the active power p.

Active power p and reactive power q have small oscillations due to switching deadtime and errors in the current control loops.

2) Case 2—Strategy 1 in a Four-Wire Topology (Losses Minimization With Ripple-Free Torque Restriction): Measured currents in abc variables, which are necessary to obtain the constant total power P_T, are shown in Fig. 6(a).

Fig. 6(b) shows the waveforms of the power components for this case. It can be observed that, as a result of applying the proposed control strategy, the reactive power q is null.

It can be also observed in Fig. 6(b) that the homopolar power p_0 presents an oscillatory component. This power added to the active power p, which also has an oscillatory component, results in a constant total power $P_T = 1.05$ p.u. higher than the active power p. Once again, the active power p and reactive power q present small oscillations due to switching deadtime and errors in the current control loops.

It is important to remark that the total power in Case 2 is 2% greater than that in Case 1, which demonstrates that by controlling the homopolar current, an additional energy can be generated.

Even for homopolar power p_0 and active power p with oscillatory components, the total power P_T remains constant, which implies that at constant speed, the generated torque is constant.

3) Case 3—Strategy 2 in a Three-Wire Topology (Maximization of the Total Power With Thermal Limit Restriction): In Fig. 7(a), measured currents in abc variables can be observed. These currents are necessary to obtain the maximum total power P_T.

The waveforms of the power components for this case are shown in Fig. 7(b). The reactive power q is null as a result of applying the proposed control strategy, and the homopolar power p_0 is null due to the fact that the neutral is not connected. In this case, the active power p shows an oscillatory component,

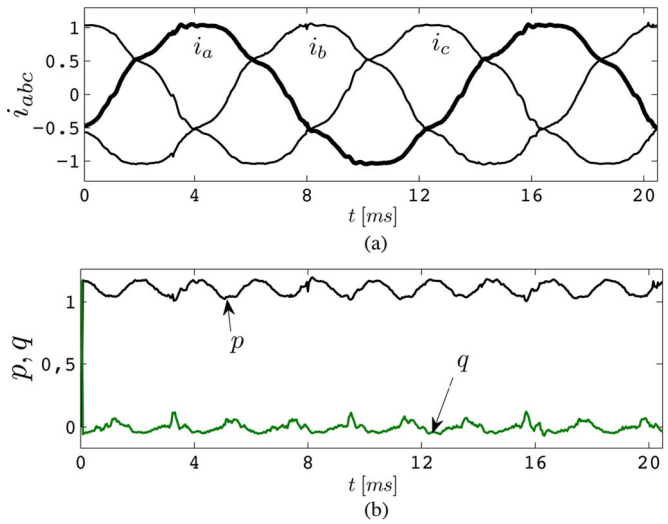

Fig. 7. Currents and power components for Case 3: Strategy 2 and three-wire topology (experimental data). (a) Measured currents. (b) Power components.

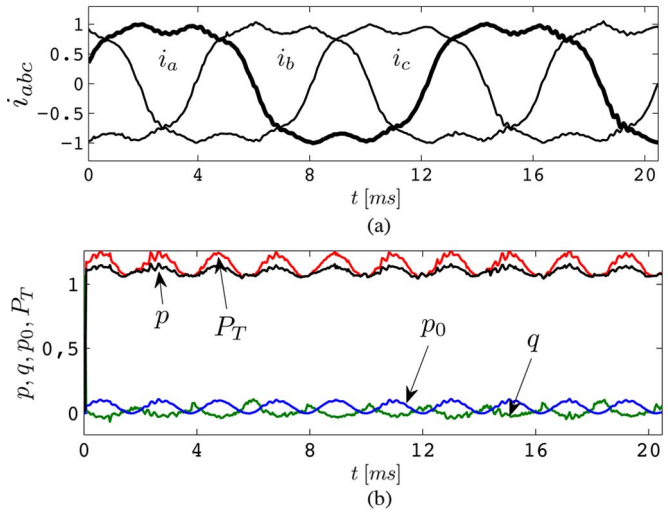

Fig. 8. Currents and power components for Case 4: Strategy 2 and four-wire topology (experimental data). (a) Measured currents. (b) Power components.

and therefore, the total power P_T presents one, too. This power oscillation produces torque ripple on the generator shaft, which may be harmful to the mechanical system as a whole.

4) Case 4—Strategy 2 in a Four-Wire Topology (Maximization of the Total Power With Thermal Limit Restriction): Measured currents in abc variables, which are necessary to obtain the maximum total power P_T, are shown in Fig. 8(a). It can be seen that the current waveform tends to a square shape when the generated power is higher.

Fig. 8(b) shows the waveforms of the power components for this case. As in the previous cases, it can be observed that as a result of applying the proposed control strategy, the reactive power q is null. It can be also observed that both the homopolar power p_0 and the active power p present oscillatory components like in Case 2. The addition of both results in a total power P_T with the highest average value of all cases. However, unlike Case 2, the total power presents an oscillatory component.

It is important to remark that the total power in Case 4 is 4% greater than that in Case 3 and 7% grater than that with block commutation, which demonstrates that by controlling the zero-sequence current, an additional energy can be generated.

TABLE II
EXPERIMENTAL RESULTS

Case \ Power in p.u.	Average P_T	Ripple Δ_{PP}
Ideal Block Commutation	1	–
Strategy 1 / 3-wire	1.03	0
Strategy 1 / 4-wire	1.05	0
Strategy 2 / 3-wire	1.03	0.118
Strategy 2 / 4-wire	1.07	0.136

B. Comparative Analysis of the Study Cases

Table II summarizes the experimental results presented in the previous section. The proposed strategies were applied to the IVS4500 generator, and the resulting total mean power and the torque ripple are presented. The rated power using the standard block commutation was calculated for the rated losses. No ripple was calculated for this case, as an ideal commutation was considered. All cases produce the same losses due to the Joule effect in the windings.

The machine was driven at constant speed. Consequently, the torque was calculated as the ratio between the generated instantaneous power P_T and the rotor angular speed ω.

The results summarized in Table II are for a given, for us available, machine. However, it should be remarked that the power gain depends on the waveform of the EMF. A waveform that is nearer to a square shape would provide higher gains.

Machines with trapezoidal EMF and controlled with block commutation present higher torque density than machines with sinusoidal EMF and sinusoidal current waveforms [7]. In the present paper, this advantage is raised even more by the proposed algorithm.

The standard block commutation that is taken as a basis of comparison also produces torque ripple [7]. Usually, the torque ripple is filtered by the inertia of the generator. In most cases, it is even very difficult to measure the torque ripple [28]. However, the influence on the system performance, as, for instance, in wind energy systems, depends on the system and cannot be well pondered by the authors.

V. CONCLUSION

The main hypothesis proposed in this paper is that by controlling the stator currents, including the harmonic and zero-sequence components, of a nonsinusoidal PMG, additional energy can be obtained without increasing losses.

Two different control strategies were proposed: The first strategy aims at minimizing losses applying ripple-free torque restriction. The second strategy aims at maximizing the total power applying thermal limit restriction.

These two strategies were implemented in three- and four-wire topologies; therefore, four different cases were analyzed and implemented in an experimental system specially built to validate these proposals.

Strategy 1 is intended to extract continuous power from the generator shaft while minimizing losses due to the Joule effect in its windings.

Strategy 2 is intended to extract the maximum mean power (disregarding ripple) from the generator, keeping the Joule losses at a constant value and equal to the generator nominal losses.

For the available PMG, the power gain obtained by taking advantage of the harmonic components without using the zero-sequence components (three-wire system) is 3% with respect to the conventional block commutation. By taking advantage of the harmonic and the zero-sequence components (four-wire system), the gain is 5% for Strategy 1 and 7% for Strategy 2.

The power gain depends on the waveform of the EMF. Consequently, a machine could be designed with the aim of maximizing this gain. Such a machine should have an almost rectangular-shaped EMF waveform.

Finally, it is proved that Strategy 2 allows extracting more mean power than Strategy 1, but it presents the disadvantage of generating an oscillatory power and, consequently, a torque ripple on the PMG shaft. Depending on the application, the torque ripple can be filtered by the system inertia.

REFERENCES

[1] M. Liserre, T. Sauter, and J. Hung, "Future energy systems: Integrating renewable energy sources into the smart power grid through industrial electronics," *IEEE Ind. Electron. Mag.*, vol. 4, no. 1, pp. 18–37, Mar. 2010.

[2] J. Chen, J. Chen, and C. Gong, "On optimizing the aerodynamic load acting on the turbine shaft of PMSG-based direct-drive wind energy conversion system," *IEEE Trans. Ind. Electron.*, vol. 61, no. 8, pp. 4022–4031, Aug. 2014.

[3] K. Ahsanullah, R. Dutta, and M. Rahman, "Distributed and concentrated winding interior PM synchronous machine (IPMSM) for direct drive wind turbine," in *Proc. IEEE IECON/IECON*, Nov. 2013, pp. 2762–2767.

[4] F. Blaabjerg, M. Liserre, and K. Ma, "Power electronics converters for wind turbine systems," *IEEE Trans. Ind. Electron.*, vol. 48, no. 2, pp. 708–719, Mar./Apr. 2012.

[5] F. Blaabjerg and K. Ma, "Future on power electronics for wind turbine systems," *IEEE J. Emerg. Sel. Topics Power Electron.*, vol. 1, no. 3, pp. 139–152, Sep. 2013.

[6] T. Jahns and W. Soong, "Pulsating torque minimization techniques for permanent magnet ac motor drives—A review," *IEEE Trans. Ind. Electron.*, vol. 43, no. 2, pp. 321–330, Apr. 1996.

[7] D. Dorrell *et al.*, "A review of the design issues and techniques for radial-flux brushless surface and internal rare-earth permanent-magnet motors," *IEEE Trans. Ind. Electron.*, vol. 58, no. 9, pp. 3741–3757, Sep. 2011.

[8] K. Jezernik, R. Horvat, and M. Curkovic, "A switching control strategy for the reduction of torque ripple for PMSM," *IEEE Trans. Ind. Informat.*, vol. 9, no. 3, pp. 1272–1279, Aug. 2013.

[9] Y. Kim, Y. Choi, and J. Lee, "Speed-sensorless vector control for permanent-magnet synchronous motors based on instantaneous reactive power in the wide-speed region," in *Proc. Inst. Elect. Eng.—Elec. Power Appl.*, vol. 152, no. 5, Sep. 2005, pp. 1343–1349.

[10] S.-J. Park, H.-W. Park, M. H. Lee, and F. Harashima, "A new approach for minimum-torque-ripple maximum-efficiency control of BLDC motor," *IEEE Trans. Ind. Electron.*, vol. 47, no. 1, pp. 109–114, Feb. 2000.

[11] H. Zhu, X. Xiao, and Y. Li, "Torque ripple reduction of the torque predictive control scheme for permanent-magnet synchronous motors," *IEEE Trans. Ind. Electron.*, vol. 59, no. 2, pp. 871–877, Feb. 2012.

[12] C. Xia, Y. Xiao, W. Chen, and T. Shi, "Torque ripple reduction in brushless dc drives based on reference current optimization using integral variable structure control," *IEEE Trans. Ind. Electron.*, vol. 61, no. 2, pp. 738–752, Feb. 2014.

[13] G.-H. Lee, S.-I. Kim, J.-P. Hong, and J.-H. Bahn, "Torque ripple reduction of interior permanent magnet synchronous motor using harmonic injected current," *IEEE Trans. Magn.*, vol. 44, no. 6, pp. 1582–1585, Jun. 2008.

[14] P. Kshirsagar and R. Krishnan, "High-efficiency current excitation strategy for variable-speed nonsinusoidal back-EMF PMSM machines," *IEEE Trans. Ind. Appl.*, vol. 48, no. 6, pp. 1875–1889, Nov. 2012.

[15] H. Geng, D. Xu, B. Wu, and G. Yang, "Active damping for PMSG-based WECS with dc-link current estimation," *IEEE Trans. Ind. Electron.*, vol. 58, no. 4, pp. 1110–1119, Apr. 2011.

[16] H. Akagi, E. H. Watanabe, and M. Aredes, *Instantaneous Power Theory and Applications to Power Conditioning*. Piscataway, NJ, USA: IEEE Press, 2007.

[17] R. Leidhold, G. Garcia, and E. H. Watanabe, "PMAC motor control strategy, based on the instantaneous active and reactive power, for ripple-torque and copper-losses minimization," in *Proc. IEEE IECON/IECON*, 2000, vol. 2, pp. 1401–1405.

[18] F. Scuiller, "Magnet shape optimization to reduce pulsating torque for a 5-phase PM low speed machine," *IEEE Trans. Magn.*, vol. 50, no. 4, pp. 1–9, Apr. 2014.

[19] R. O. C. Lyra and T. Lipo, "Torque density improvement in a six-phase induction motor with third harmonic current injection," *IEEE Trans. Ind. Appl.*, vol. 38, no. 5, pp. 1351–1360, Sep./Oct. 2002.

[20] E. Levi, "Multiphase electric machines for variable-speed applications," *IEEE Trans. Ind. Electron.*, vol. 55, no. 5, pp. 1893–1909, May 2008.

[21] F. Meinguet, E. Semail, and J. Gyselinck, "Enhanced control of a PMSM supplied by a four-leg voltage source inverter using the homopolar torque," in *Proc. IEEE ICEM*, Sep. 2008, pp. 1–6.

[22] S. Bolognani, M. Zordan, and M. Zigliotto, "Experimental fault-tolerant control of a PMSM drive," *IEEE Trans. Ind. Electron.*, vol. 47, no. 5, pp. 1134–1141, Oct. 2000.

[23] B. Welchko, T. Lipo, T. Jahns, and S. Schulz, "Fault tolerant three-phase ac motor drive topologies: A comparison of features, cost, and limitations," *IEEE Trans. Power Electron.*, vol. 19, no. 4, pp. 1108–1116, Jul. 2004.

[24] N. Freire and A. Marques Cardoso, "A fault-tolerant direct controlled PMSG drive for wind energy conversion systems," *IEEE Trans. Ind. Electron.*, vol. 61, no. 2, pp. 821–834, Feb. 2014.

[25] G. Catuogno, D. Forchetti, G. Garcia, and R. Leidhold, "Power flow control with losses minimization and fault tolerance for PMSG," in *Proc. IEEE IECON*, Oct. 2012, pp. 3566–3571.

[26] K. Wang, Z. Zhu, G. Ombach, and W. Chlebosz, "Average torque improvement of interior permanent-magnet machine using 3rd harmonic in rotor shape," *IEEE Trans. Ind. Electron.*, vol. 61, no. 9, pp. 5047–5057, Sep. 2014.

[27] D. P. Bertsekas, *Constrained Optimization and Lagrange Multiplier Methods*. Belmont, MA, USA: Athena Scientific, 1996.

[28] G. Heins, M. Thiele, and T. Brown, "Accurate torque ripple measurement for PMSM," *IEEE Trans. Instrum. Meas.*, vol. 60, no. 12, pp. 3868–3874, Dec. 2011.

Guillermo R. Catuogno (S'09) was born in Villa Mercedes, Argentina, in 1981. He received the Electrical and Electronics Engineering degree from the Universidad Nacional de San Luis, San Luis, Argentina, in 2007, and the Doctorate of Engineering degree from the Universidad Nacional de Río Cuarto, Río Cuarto, Argentina, in 2013.

Since 2008, he has been with the Grupo de Electrónica Aplicada, Universidad Nacional de Río Cuarto. He is also with the Consejo Nacional de Investigaciones Científicas y Técnicas, Buenos Aires, Argentina. His research interests include electric generator control, permanent-magnet synchronous machines, and renewable energy generation.

Daniel G. Forchetti was born in Rosario, Argentina, in 1975. He received the Electrical Engineer degree from the Universidad Nacional de Río Cuarto, Río Cuarto, Argentina, in 1999, and the Doctor of Engineering degree from the Universidad Nacional de La Plata, La Plata, Argentina, in 2010.

Since 1996, he has been with the Grupo de Electrónica Aplicada, Universidad Nacional de Río Cuarto. He is also with the Consejo Nacional de Investigaciones Científicas y Técnicas, Buenos Aires, Argentina. His research interests include electric generator control, sensorless induction machine control, and renewable energy generation.

Roberto Leidhold (S'94–M'03) received the B.S. degree in electronics engineering from the Universidad Nacional de Cordoba, Cordoba, Argentina, in 1995; the M.S. degree from the Universidad Nacional de Río Cuarto, Río Cuarto, Argentina, in 2000; and the Ph.D. degree from the Universidad Nacional de La Plata, La Plata, Argentina, in 2003.

From 2003 to 2004, he was Postdoctoral Fellow with the Universidad Nacional de Río Cuarto. From 2005 to 2011, he was with the Technical University of Darmstadt, Darmstadt, Germany, first as a Research Scholar of the Alexander von Humboldt Foundation, then as a Research Associate, and later as a Principal Investigator. Since 2011, he has been a Professor of Electric Drive Systems with the Otto-von-Guericke-Universitaet Magdeburg, Magdeburg, Germany. His research interests include control of drives, electric machines, and renewable energy generation.

Guillermo O. Garcia (M'86–S'90–M'95–SM'01) was born in Río Cuarto, Argentina, in 1954. He received the Electrical and Electronics Engineering degree from the Universidad Nacional de Córdoba, Córdoba, Argentina, in 1981, and the M.Sc. and Ph.D. degrees in electrical engineering from the Universidade Federal do Rio de Janeiro, Rio de Janeiro, Brazil, in 1990 and 1994, respectively.

Since 1994, he has been with the Universidad Nacional de Ro Cuarto, Ro Cuarto, Argentina, where he is currently the Director of the Grupo de Electrónica Aplicada. He is also with the Consejo Nacional de Investigaciones Científicas y Técnicas, Buenos Aires, Argentina. His research interests include power electronics, electric vehicles, and renewable energy conversion.